



ERNEST ORLANDO LAWRENCE BERKELEY NATIONAL LABORATORY

Exterior Exposed Ductwork: Delivery Effectiveness and Efficiency

Wm. Woody Delp, Nance Matson,
and Mark P. Modera
**Environmental Energy
Technologies Division**

July 1996



REFERENCE COPY |
Does Not |
Circulate |
Bldg. 50 Library - Ref.
Lawrence Berkeley National Laboratory

DISCLAIMER

This document was prepared as an account of work sponsored by the United States Government. While this document is believed to contain correct information, neither the United States Government nor any agency thereof, nor the Regents of the University of California, nor any of their employees, makes any warranty, express or implied, or assumes any legal responsibility for the accuracy, completeness, or usefulness of any information, apparatus, product, or process disclosed, or represents that its use would not infringe privately owned rights. Reference herein to any specific commercial product, process, or service by its trade name, trademark, manufacturer, or otherwise, does not necessarily constitute or imply its endorsement, recommendation, or favoring by the United States Government or any agency thereof, or the Regents of the University of California. The views and opinions of authors expressed herein do not necessarily state or reflect those of the United States Government or any agency thereof or the Regents of the University of California.

Exterior Exposed Ductwork:
Delivery Effectiveness and Efficiency*

Wm. Woody Delp
Nance Matson
Mark P. Modera

Energy and Performance of Buildings Group
Energy and Environment Division
Ernest Orlando Lawrence Berkeley National Laboratory
University of California
Berkeley, CA 94720

July 1996

* This work was supported by the California Institute for Energy Efficiency, under Contract B93-05A, and the Assistant Secretary for Energy Efficiency and Renewable Energy, Office of Building Technology of the U.S. Department of Energy, under Contract No. DE-AC03-76SF00098.

Exterior Exposed Ductwork: Delivery Effectiveness and Efficiency*

Wm. Woody Delp, Nance E. Matson and Mark P. Modera

Energy Performance of Buildings Group

Energy and Environment Division

Lawrence Berkeley National Laboratory

April 9, 1997

Abstract

Most of California's light commercial buildings use air transport through ductwork for thermal distribution. The same air distribution systems are often used to provide both thermal comfort and ventilation for these buildings. Some air distribution ductwork is installed on rooftops, exposed directly to the outside environment. As such, there exist potential energy penalties related to externally installed ductwork. In order to evaluate the magnitude of these penalties, a case study was conducted of a one-story community college building, located in California's Sacramento Valley. The majority of the building's air distribution ductwork was located on the roof. Energy-related issues studied in this case included duct-related thermal losses (duct leakage and conduction), delivery effectiveness and efficiency, thermal comfort issues and the effect of a roof retrofit (additional insulation and a reflective coating). The building in this study underwent a retrofit project involving additional insulation and a highly reflective coating applied to the roof and ducts. As part of this project, methods were developed to analyze the air distribution system effectiveness independent of the introduction of outside air through an outside air damper. A simplified model was developed to predict the effectiveness and efficiency of the distribution system. The time frame of the retrofit allowed two separate three week monitoring periods, pre and post-retrofit, during the summer of 1995. Despite the fact that the ducts started off with a conduction efficiency of 97%, the delivery efficiency was on average only 73% (with a supply side effectiveness of 78% and return effectiveness of 92%). This is due to the losses from the ducts being located on the roof. The retrofit increased the delivery efficiency to an average of 89% (with a supply side effectiveness of 90% and return effectiveness of 99%), reducing the average energy use for conditioning by 22%. The model predicted, on average, the results within 10%, or better, of measured results.

1.0 Introduction

The majority of California's commercial buildings have thermal distribution systems. It is estimated that 63%¹ of these distribution systems are air-based and use ductwork distribution networks [Modera et al 1996]. Thermal distribution ductwork systems used in small commercial buildings are similar to those used in residential construction and are subject to the same kinds of leakage and conduction loss issues. The extent and impact of the duct-related thermal losses depends directly on the location of the ductwork. For ducts located entirely within the conditioned space, any thermal losses go directly to the conditioned space. The greatest thermal losses and related energy penalties occur when ducts are located entirely outside of the building envelope. Factors affecting thermal losses and energy penalties of exterior ducts include leakage and conduction losses, direct solar radiation effects and solar reflection effects. In addition to impacting the energy efficiency of a thermal distribution system, differences in the lengths of exterior duct runs can affect the temperature of the air delivered to the space at the registers. Where long duct runs are exposed to high temperature environments, such as on a roof during cooling conditions, the supply air can experience significant temperature rise before the registers. In areas served by long duct runs, this effect directly impacts the thermal comfort and results in uneven temperature distributions within the building.

One way by which commercial-building systems differ from residential systems is that they are often used to provide ventilation as well as space conditioning. In residences the passive method of infiltration and operable windows is typically used along with intermittent bathroom and kitchen exhaust fans operated by occupants to remove cooking smells, moisture, etc. Recently, active fan-based whole house ventilation systems have begun to be installed on a limited basis, where the central thermal distribution system is used to bring outside air into the house via an outside air duct. This active method is similar to the strategies used in commercial buildings. Most of California's commercial buildings use a single ductwork distribution system to provide thermal comfort and ventilation to a space. Outside air is introduced into the return air section of a commercial building's system using an arrangement of outside air openings and dampers. Economizers can also be present, providing ventilative cooling using the requisite dampers, outside air inlets and barometric reliefs. Traditionally, return duct leakage is measured based on the whole return system, from the return grille to the boundary between the return plenum and the fan in the air handling unit. Economizers or outside air openings are intentional "holes" which appear as large leakage sites contributing to the overall leakage of the return system. In order to take this into account, a new calculation methodology has been developed which separates out the openings from the unintentional leakage.

1. 63% of individual systems were positively reported as having some form of air based thermal distribution, while 29% of the systems were grouped into a single none/not known category.

To look at these and other energy issues related to exterior exposed ductwork, a case study was conducted at a building on the campus of a community college located in Sacramento, California. The majority of the distribution systems' ductwork was located on the roof, providing an excellent opportunity to evaluate the effect of duct leakage, conduction losses, solar radiation and the application of roof insulation and reflective coating on the energy performance, delivery effectiveness and efficiency of the duct system. This paper presents the findings of this case study, as well as the model and analysis methodology used to evaluate the performance of the system.

2.0 Building Description

The building in this study contains classroom, laboratory and office space and is part of a community college located in Sacramento, California. The single story brick building has a flat concrete roof, was constructed in the 1950s and has a total floor area of approximately 2,000 m² (21,500 ft²). The building is located on the south end of campus with a major street to the south and parking lots to the east. There is essentially no shading from the south or the east. The west side of the building is lightly shaded by some trees.

2.1 HVAC Systems

A centralized chiller plant serves the building studied as well as an adjacent building, providing chilled water to individual air handlers and fan coil units. The building originally had ducted fan-coil units and ductless through-the-wall fan coil units located in ceiling cavities, storage rooms, and closets. Due to a history of complaints regarding unsatisfactory performance of the HVAC systems, the building's systems were completely retrofitted in the early 1980s. The HVAC retrofit included installing fifteen roof-mounted constant-volume air-handling units with chilled-water coils, and air-side economizers. In order to respond directly to the load in the space served, each unit has the ability to vary the water flow rate through its chilled water coil. The total available cooling capacity of the units is 233 kW (66 tons). The combined supply-air flow for all of the air handlers at design is 53,300 m³/hr (31,300 cfm). The combined design outside air flow, via outside air grilles on the rooftop air handlers, is 10,900 m³/hr (6,400 cfm). The outside air grilles are fixed without any provision to adjust the air flow. During non-economizer operation, the systems do not have any provisions for exhausting stale air from the building. As a result, the systems pressurize the building. Correspondingly, the position of internal and external doors throughout the building assist in the circulation and exhaust of building air and directly affect building pressurization which affects the actual volume of outside air pulled through the outside air grilles and delivered to the space by each system.

For the most part, ductwork installed for the new systems was placed on the roof. Existing ductwork was modified and reused in some spaces which had hard plaster ceilings. Figure 1 shows a typical cross-section detail for the ductwork located on the roof. The ducts are elevated approximately 0.5 m above the roof deck and run horizontally from the air handler across the roof deck. The majority of the ductwork (approximately 75% of the total length) is located on the roof. The ducts drop down through the roof deck at each branch take-off, terminating at ceiling registers.

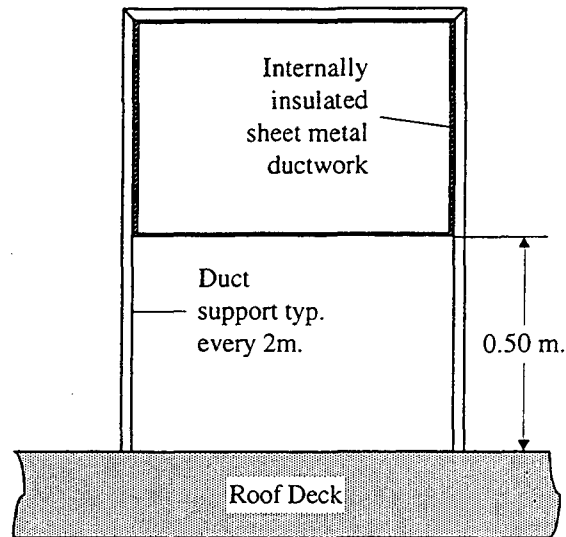


FIGURE 1. Typical exposed duct detail

2.2 “Cool-Roof” Retrofit

During the summer of 1995, the Sacramento Municipal Utility District (SMUD) conducted a “Cool-Roof” retrofit at the building. This retrofit was carried out based on information gathered during the “Cool-Roof” research projects conducted by SMUD and LBNL [Akbari et al 1993]. The “Cool-Roof” research projects evaluated the thermal impact of improving the roof deck insulation and changing the surface properties of buildings. The large exposed unshaded flat roof of this building provided good savings opportunities. For the “Cool-Roof” retrofit on this building, a spray-applied expanding closed-cell polyurethane ($R\text{-value} = 0.433 \text{ m}^2 \cdot \text{K}/\text{W} \cdot \text{cm}$) was applied. Exposed ductwork received 1.2 to 1.7 cm of insulation, and the roof 10 to 15 cm. It was believed that the insulation sprayed on the ductwork would also seal any leaks present in the ductwork. After applying the insulation, a highly reflective coating (manufacturer claimed reflectivity of 85%) was applied to the roof and any external ductwork. The ductwork was a secondary consideration in the cool roof retrofit. As a result, only the top and sides of the ducts were sprayed, leaving the underside of the ductwork, facing the roof deck, unchanged.

2.3 System Studied

One of the building’s air handler systems, serving a lecture hall (floor area = 147 m^2 ($1,580 \text{ ft}^2$)), was selected for detailed study. Figure 2 shows the lecture hall, the associated air handler and corresponding ductwork. The lecture hall has a seating capacity of 120 people and is used for both day

and evening classes. This space has a single exterior door and a double door to an internal hallway, but no exterior windows. All of the ductwork for this system is located on the roof with no solar shading

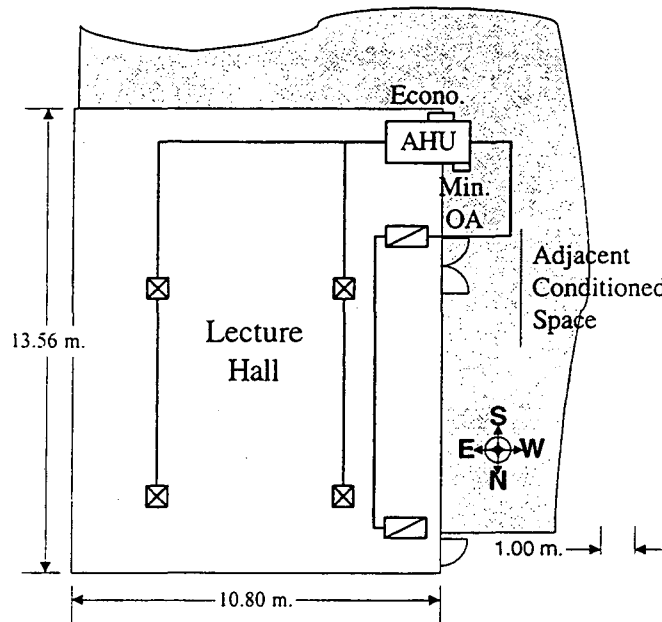


FIGURE 2. Layout of HVAC distribution for lecture hall

The air handling unit studied has a cooling capacity of 28 kW (8 ton), a design fan-flow rate of 5,100 m³/h (3,000 cfm), and a design outside air flow rate of 2,125 m³/h (1,250 cfm). The breakdown of the loads is approximately 50% due to the outside air, 40% due to internal loads (120 people), and 10% due to the building shell. Since 50% of the cooling capacity is for the outside air load, this leaves the remaining half of the cooling capacity, essentially a useful design capacity of 14 kW (4 ton), to take care of the space's internal and building shell loads.

3.0 Data Collection

The primary goals of the monitoring work were to 1) determine the air flow and thermal impact of duct losses through conduction and leakage losses and 2) determine the changes in thermal losses attributable to the “Cool-Roof” retrofit project. This required a two-phase data collection process, before and after the retrofit project. Data collection consisted of both one-time diagnostic measurements, for values that did not change with time, and a period of continuous monitoring, for values that were time dependent. The diagnostic and monitoring data collected was used to determine energy delivery rates, thermal energy losses and overall efficiencies.

3.1 Diagnostic Measurements

Diagnostic measurements consisted of noting certain physical system parameters (location and capacity of the equipment, size and thermal properties of the ductwork, etc.) and measuring air flows. Table 1 shows the results of the diagnostic measurements, including system air flows, system duct leakage and the effects of the “Cool-Roof” retrofit activities

System Duct Leakage. Supply duct leakage was measured as the difference between the fan flow and the sum of flows at the supply registers. Return duct leakage was measured as the difference between the fan flow and the sum of the flows at the return grilles and the outside air grille. The ducts had been “sealed” with mastic at a previous point in time. As such, the amount of the overall system’s pre-retrofit duct leakage was lower than the resolution of our measurement techniques (115 m³/h (68 cfm) supply, -216 m³/h (-127 cfm) return). The apparent pre-retrofit return duct leakage is negative but is within the measurement resolution. It can be assumed that the return ducts were tight. The retrofit included applying exterior insulation and reflective coating to the rooftop ductwork. The leakage was not changed by the retrofit. The repeatability of the fan flow measurements was within 3%, which is the same as for the other flows discussed.

System Air Flows. The system air flows measured included flows across the system fan, supply grilles, return grilles and the outside air inlet grille. Grille and outside air inlet flow measurements were made with a flow capture method using a flow hood coupled to a calibrated fan, where the fan acts as a flow metering device. The pressures in the duct remained the same with or without the flow hood in place, indicating that the measurement method and set-up did not significantly affect the total air flow being measured. The fan coupled to the flow hood was operated to maintain this pressure. Fan flow measurements were made using the constant injection tracer gas technique described in Appendix A. The repeatability of all flow measurements are within 3% of the measured values.

Outside Air Flows. Outside air delivery did not meet the design requirements, nor would it be able to meet the minimum recommended outside air delivery suggested in ASHRAE Standard 62-1989 [ASHRAE 1989a]. This is due to the fact that no explicit exhaust method exists for the building, and therefore outside air (OA) flowrates are limited by the pressure in the space. The higher the pressure in the space, the lower the amount of outside air flowing into the system through the outside air grilles on the rooftop air handling units. The presence of exhaust fans or intentional/unintentional openings in the building shell would result in a lower pressure in the space and, correspondingly, more outside air would be pulled into the space through the outside air grilles. In this building, the old through-the-wall fan coil units were abandoned but left in place during the HVAC system retrofit of the early 1980s. Significant air flowrates out of the building were observed across the outside air grilles on these units. The positioning of interior hallway and exterior doors also affected the amount of outside air delivered to the space. This sensitivity, observed during the diagnostic measurements, did not affect the total air flow across the system fan. Rather, it affected the proportion of air entering the system airstream through the outside air grille versus through the return grilles in the space. This resulted in the air flow into the return registers and outside air grilles being very dependent on the position of the doors.¹

Duct Insulation and Conduction Efficiency. Conduction efficiency, β , is a measure of the temperature change of air flowing through a duct. It is the ratio of the temperature difference of the air in the duct and its surroundings at the end of the duct and the same difference at the beginning of the duct. For an ideally insulated duct this will be unity, all real ducts will be less. By solving a basic heat transfer equation, β can be related to the air flow rate, surface area, and thermal resistance of the duct (See Appendix B). Prior to the "Cool-Roof" retrofit, the calculated conduction efficiency was 96.9%. After doubling the exterior duct insulation from R-4 to R-8 ($^{\circ}\text{F}\cdot\text{ft}^2\cdot\text{h}/\text{btu}$), β increased to 98.5%, an increase of 1.7% of the original value.

1. With doors open, the OA flow increases and the return register decreases by the same amount. This was measured under a single condition, the actual results are dependent on both wind conditions and door positions in the rest of the building, neither of which we had control over during both the diagnostic or monitoring periods. An additional measurement was made with the OA opening blocked; the return register flows increased by the same amount which was entering the OA grille. This finding suggests the return side is dependent on the wind and door positions, but it does not change the supply delivery rates.

TABLE 1. Diagnostic Results

	Design	Pre-Retrofit	Post-Retrofit
System Duct Leakage:			
Supply Leakage m ³ /h (cfm)	-----	115 (67)	-1 (0)
Supply Leakage (% of Fan Flow)	-----	2.2%	0.0
Return Leakage ^a m ³ /h (cfm)	-----	-216 (-127)	47 (28)
Return Leakage (% of Fan Flow)	-----	-4.2%	0.9%
System Air Flow Rates:			
Fan Flow m ³ /h (cfm)	5,100 (3,000)	5,157 (3,033)	5,122 (3,013)
Supply 1 m ³ /h (cfm)	1,275 (750)	1,515 (891)	1,465 (862)
Supply 2 m ³ /h (cfm)	1,275 (750)	1,124 (661)	1,226 (721)
Supply 3 m ³ /h (cfm)	1,275 (750)	1,351 (794)	1,425 (838)
Supply 4 m ³ /h (cfm)	1,275 (750)	1,052 (619)	1,007 (592)
Total supply m ³ /h (cfm)	5,100 (3,000)	5,042 (2,966)	5,123 (3,013)
Return 1 m ³ /h (cfm)	1,488 (875)	2,381 (1,401)	2,295 (1,350)
Return 2 m ³ /h (cfm)	1,488 (875)	1,647 (969)	1,576 (927)
Total Return m ³ /h (cfm)	2,975 (1,750)	4,028 (2,370)	3,871 (2,277)
Outside Air (OA) Inlet m ³ /h (cfm)	2,125 (1,250)	1,344 (791)	1,203 (708)
OA Delivery ^b (% of Design)	-----	62%	57%
“Cool-Roof” Retrofit Effects:			
Duct R-value (°F-ft ² -h/btu)	-----	4	8
β ^c (Conduction Efficiency)	-----	0.969	0.985

^aReturn Leakage = Fan Flow - (Total Return + OA Inlet)

^b(OA Inlet * Fraction of Supply Air Entering the Space)/ OA Design

^cβ = (T_{outlet} - T_∞) / (T_{inlet} - T_∞)

3.2 Short-term Monitoring

Short-term monitoring, including temperature and solar radiation measurements, took place over two separate three-week periods during the summer months of 1995. These two periods represented the pre- and post-retrofit conditions and operational patterns of the building's HVAC system. The weather conditions and space utilization were similar during both periods. The average ambient daytime outside temperatures were 28.2°C (pre-retrofit) and 27.9°C (post-retrofit). The average artificial sol-air temperatures (see section 4.1) were 37.5°C (pre-retrofit) and 37.6°C (post-retrofit).

Temperature and incident solar radiation measurements were recorded every 90 seconds during each three-week monitoring period. Temperature measurements were taken at all four supply registers,

both return registers, the supply plenum (an averaged traverse of four sensors), the return plenum (two locations, middle and end), two locations on the supply duct surface, two locations on the return duct surface, the roof surface and the ambient outside air with a shielded and aspirated thermistor. The calibration accuracy of the temperature measurements were within 0.1°C, while the solar radiation measurements were within 3%.

4.0 Analysis and Results

The intention of this analysis was to determine the thermal comfort, and energy impact relating to locating the HVAC system's ductwork on the roof and outside of the conditioned space. This analysis focuses on quantifying the magnitude of the conduction losses and the effect of direct and reflected solar radiation on the ducts, the delivery effectiveness and efficiency, the effect of the "Cool-Roof" retrofit on system performance and thermal comfort issues. A simplified model that can be used to evaluate the effectiveness and efficiency of the delivery system was verified using measurement and model results.

4.1 Sol-Air Temperature and Conduction Losses

Conduction losses in a duct are proportional to the temperature difference between the air in the duct and its surroundings. Since the ducts in this building are primarily located on the unshaded roof deck of the building and are exposed to solar radiation, the surface temperature of the ducts rises significantly above the outside air temperature. The sol-air temperature is the adiabatic temperature for a surface exposed to solar radiation and can be used in this analysis as an approximation of the roof and duct surfaces. The sol-air temperature, as per the ASHRAE 1989 Handbook of Fundamentals [ASHRAE 1989b], is defined in Equation 1 and is a function of the surface properties. ASHRAE suggests the following typical values for horizontal surfaces: $h_o = 17 \text{ W/m}^2 \cdot ^\circ\text{C}$, $\epsilon_{IR}\Delta R/h_o = 3.9^\circ\text{C}$, and $\alpha_{sol}/h_o = 0.0264 \text{ m}^2 \cdot ^\circ\text{C/W}$ (light colored surfaces) or $\alpha_{sol}/h_o = 0.0528 \text{ m}^2 \cdot ^\circ\text{C/W}$ (dark colored surfaces). This corresponds to an α_{sol} of 0.45 for the light surface (55% reflectivity) and 0.9 for the dark surface (10% reflectivity).

$$\text{Sol-Air} = T_\infty + \alpha_{sol}/h_o \cdot I_t - \epsilon_{IR}\Delta R/h_o \quad (1)$$

where:

T_∞ = outside air temperature: $^\circ\text{C}$ ($^\circ\text{F}$)

α_{sol} = absorptance of surface to solar radiation

h_o = combined coefficient of heat transfer: $\text{W/m}^2 \cdot ^\circ\text{C}$ ($\text{Btu} / \text{h} \cdot \text{ft}^2 \cdot ^\circ\text{F}$)

I_t = total incident radiation: W/m^2 ($\text{Btu} / \text{h} \cdot \text{ft}^2$)

ϵ_{IR} = hemispherical emittance of the surface

ΔR = difference between long-wave radiation incident on the surface from the sky and surroundings and radiation emitted by a blackbody at the outside air temperature: W/m^2 ($\text{Btu} / \text{h} \cdot \text{ft}^2$)

The sol-air temperatures, for the pre- and post-retrofit conditions, were calculated using the ASHRAE recommended values along with the measured values of the outside air temperature and total incident solar radiation. Figure 3 compares the measured roof temperatures to the calculated sol-air temperatures for light and dark surfaces. The pre-retrofit roof temperatures fall between the dark and light surface sol-air temperatures, while the post-retrofit roof temperatures agree closely with the light surface sol-air temperature.

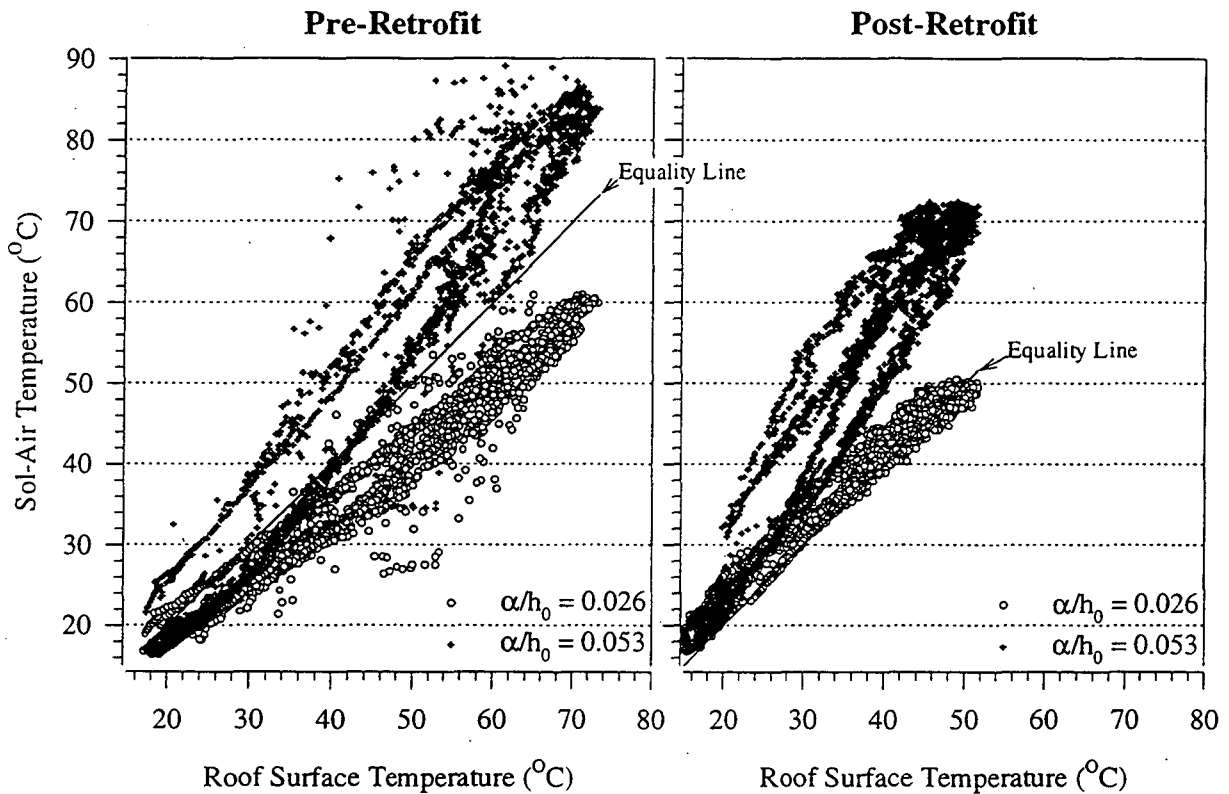


FIGURE 3. Calculated sol-air temperatures vs. measured surface temperatures

Using the measured roof surface temperature as an approximation of the sol-air temperature and assuming the ASHRAE typical values for h_o and $\epsilon_{IR}\Delta R$, Equation 1 was used to derive α_{sol} (absorptance of surface to solar radiation). The pre-retrofit roof surface absorptance was calculated to be 0.68, corresponding to a roof surface reflectivity of 32%. Using the same approach, measured pre-retrofit duct surface temperatures yielded a duct surface reflectivity of 38%. These values represent “medium color” properties, despite the fact the pre-retrofit surfaces had already been painted with a silver colored paint. The manufacturer quoted a reflectivity of 85% for the acrylic coating applied during the retrofit. Using the same calculation approach based on the ASHRAE assumptions and the measured roof surface temperature, the post-retrofit coated roof and duct surface reflectivity was

calculated to be 58%. This is in line with other measurements of similar materials used on other “Cool-Roof” projects.

For comparison of pre- to post-retrofit, the sol-air temperature can be treated solely as a function of the weather (outside temperature and solar radiation) when typical ASHRAE values are assumed for the α_{sol}/h_o and $\epsilon_{IR}\Delta R/h_o$ terms. Doing this creates an artificial sol-air temperature. Since the true sol-air temperature is surface as well as weather dependent, and the “Cool-Roof” retrofit changed these surface properties, all direct comparisons between the pre and post-retrofit time periods are made using an artificial sol-air temperature corresponding to the ASHRAE light colored surface. This assumption ensures the weather conditions are accurately compared both pre and post-retrofit. However, any calculations in the model involving a ΔT uses the actual sol-air temperature for the appropriate surface.

4.1.1 Reflected Solar Radiation on the Un-Treated Bottom of the Ducts

Qualitatively, the reflective coating made a dramatic difference on the roof. The reflectivity of the roof surface changed from 32% to 58%. Pre-retrofit surfaces were “hot to the touch” while all of the post-retrofit surfaces, with the exception of the bottom of the ducts, were not. Since the bottom of the ducts remained unchanged by the retrofit, the increased roof surface reflectivity resulted in a 81% increase in the reflected energy to the bottom of the ducts.

Prior to the pre-retrofit measurements and the retrofit itself, it was assumed that the insulation and reflective coating would be applied to the bottoms of the ducts. This was not the case and the bottoms of the ducts remained in the same condition as before the retrofit. Unfortunately, duct-bottom surface temperatures were not measured during the pre-retrofit measurement phase. The pre and post-retrofit sol-air temperatures, however, can be used to compare the general thermal conditions surrounding the bottoms of the ducts. Figure 4 shows the sol-air temperatures and the temperatures on the top (pre and post-retrofit) and bottom (post-retrofit only) of the supply ductwork. The sol-air temperatures given are calculated using the typical values for a light surface. During the pre-retrofit period, the temperature on the top surface of the ductwork peaks above the sol-air temperature while it remains below the sol-air temperature during the post-retrofit period. This finding conforms with the changed properties of the duct surface. The impact of the reflected radiation on the bottom of the duct can be seen in the post-retrofit data. During the middle part of the day, from 11:00 am to about 3:00pm, the temperature of the bottom of the duct is below the sol-air temperature. During this time period, the bottom of the duct is fully shaded by the duct itself as the solar radiation angle of incidence is steep and nearly vertical. As a result, most of the solar radiation reflecting off the roof deck will reflect straight back up to the sky and the bottom of the duct will be minimally affected. Before 11:00 am and more noticeably between 4:00 and 6:00 pm, the surface temperature at the bottom of the duct is above

the sol-air temperature. This result is due to a smaller angle of incidence, reflecting the solar radiation off the roof to the bottom of the ducts.

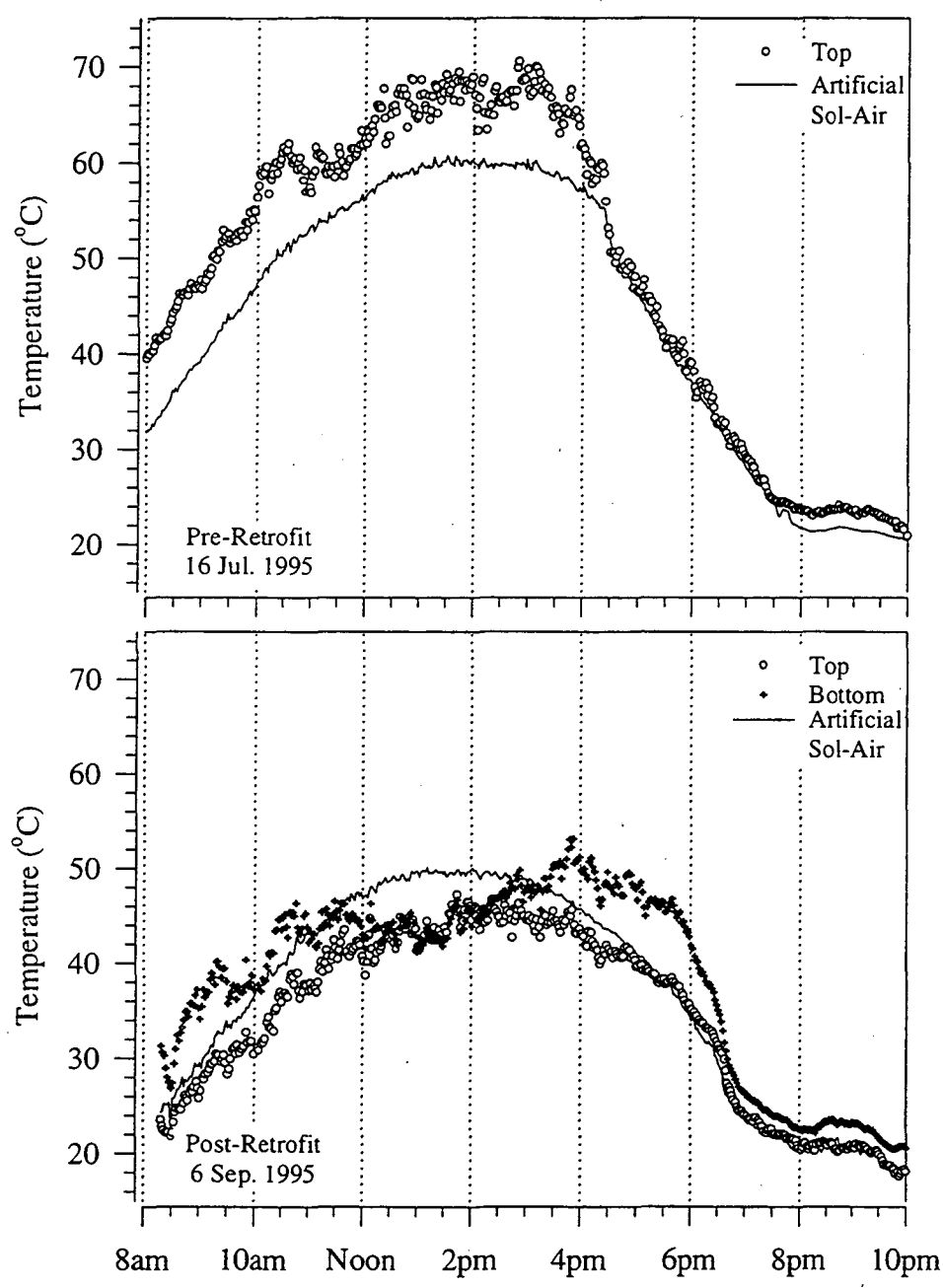


FIGURE 4. Supply duct surface temperatures: pre- and post-retrofit

4.2 Delivery Efficiency and Effectiveness

Delivery efficiency is defined as the energy supplied by the duct system at the registers divided by the energy put into the system. With traditional analysis methodologies that use the temperature change across the equipment, the effect of the introduction of outside air into the system is not taken into account. As a result, the outside-air flowrate shows up as a large return air leak and directly impacts the calculated delivery efficiency. Using this traditional method, “perfect ducts”, completely sealed with infinite thermal resistance but with an outside air source into the system, have a delivery efficiency of less than unity.

Supply and return systems can be analyzed separately by introducing the following effectiveness definitions and calculation strategies. Supply effectiveness, ϵ_s , is defined in Equation 2 as the actual capacity delivered to the space (accounting for both leakage and conduction losses) divided by the potential capacity existing at the beginning of the duct (i.e., at the supply plenum). Return losses increase the temperature of the mixed air at the return plenum and the amount of energy required to condition the air entering the return plenum. Return effectiveness, ϵ_r , is defined in Equation 3 as the minimum energy required to condition the air flowing through the return plenum divided by the actual energy. The return plenum is defined as that point just upstream of the outside-air mixing section, allowing investigation of the return system independent of any outside air that is supplied to the system. The supply and return effectiveness of perfect duct systems are equal to unity.

$$\epsilon_s = \frac{\sum_i \dot{m}_{r,i} (T_{reg,i} - T_{room})}{\dot{m}_{fan} (T_{supply} - T_{room})} \quad (2)$$

$$\epsilon_r = \frac{(T_{supply} - T_{room})}{(T_{supply} - T_{return})} \quad (3)$$

where:

$\dot{m}_{r,i}$ = flow rate of supply air leaving register i : m^3/hr (cfm)

\dot{m}_{fan} = flow rate of air through the fan: m^3/hr (cfm)

$T_{reg,i}$ = temperature of the air at register i : °C (°F)

T_{room} = room air temperature: °C (°F)

T_{supply} = supply plenum temperature: °C (°F)

T_{return} = return plenum temperature: °C (°F)

The potential capacity is defined as the capacity available at the beginning of the supply ductwork. The potential capacity in ϵ_s is equal to the minimum energy (i.e., the numerator) in ϵ_r ; therefore, the delivery efficiency (η_{del}) is obtained by simply multiplying the two effectiveness, as shown in Equation 4.

$$\eta_{del} = \epsilon_s \cdot \epsilon_r \quad (4)$$

4.2.1 Delivery Effectiveness Correlation Parameters

Several different correlation parameters were examined in order to find the best correlation parameter for use in comparing pre to post-retrofit delivery effectiveness. Four separate correlation parameter options were selected, including: outside air temperature, sol-air temperature, load factor (percent of total system capacity required to meet the space load) and the ratio of the temperature difference between the supply air and the ambient surroundings to the temperature difference between the supply air and the room ($\Delta T/\Delta T_p$). $\Delta T/\Delta T_p$ is a scaling parameter, as defined in Equation 5.

$$\frac{\Delta T}{\Delta T_p} = \frac{(T_{supply} - T_{\infty})}{(T_{supply} - T_{room})} \quad (5)$$

where:

T_{∞} = temperature of the ambient surroundings (for this case, sol-air temperature)

Figure 5 plots the supply effectiveness, ϵ_s , against the four correlation parameters. The outside air temperature shows little correlation. The sol-air temperature shows a stronger correlation than the outside air temperature alone. The model predicts a stronger correlation of ϵ_s to the load factor (LF) and the $\Delta T/\Delta T_p$ ratio. Since the system is a constant-volume system, the load factor varies considerably but it alone does not show a strong correlation with the effectiveness. The parameter $\Delta T/\Delta T_p$, which scales with the sol-air temperature and combines the ambient conditions with the load in the space, shows the strongest correlation with the delivery effectiveness. As the $\Delta T/\Delta T_p$ parameter showed the strongest correlation to the delivery effectiveness, further discussion and comparison of pre- versus post-retrofit results will use the $\Delta T/\Delta T_p$ parameter. High $\Delta T/\Delta T_p$'s are due to combinations of high

sol-air temperatures and low load factors. High sol-air temperatures represent large absolute conduction losses, and low load factors increase the relative size of these losses.

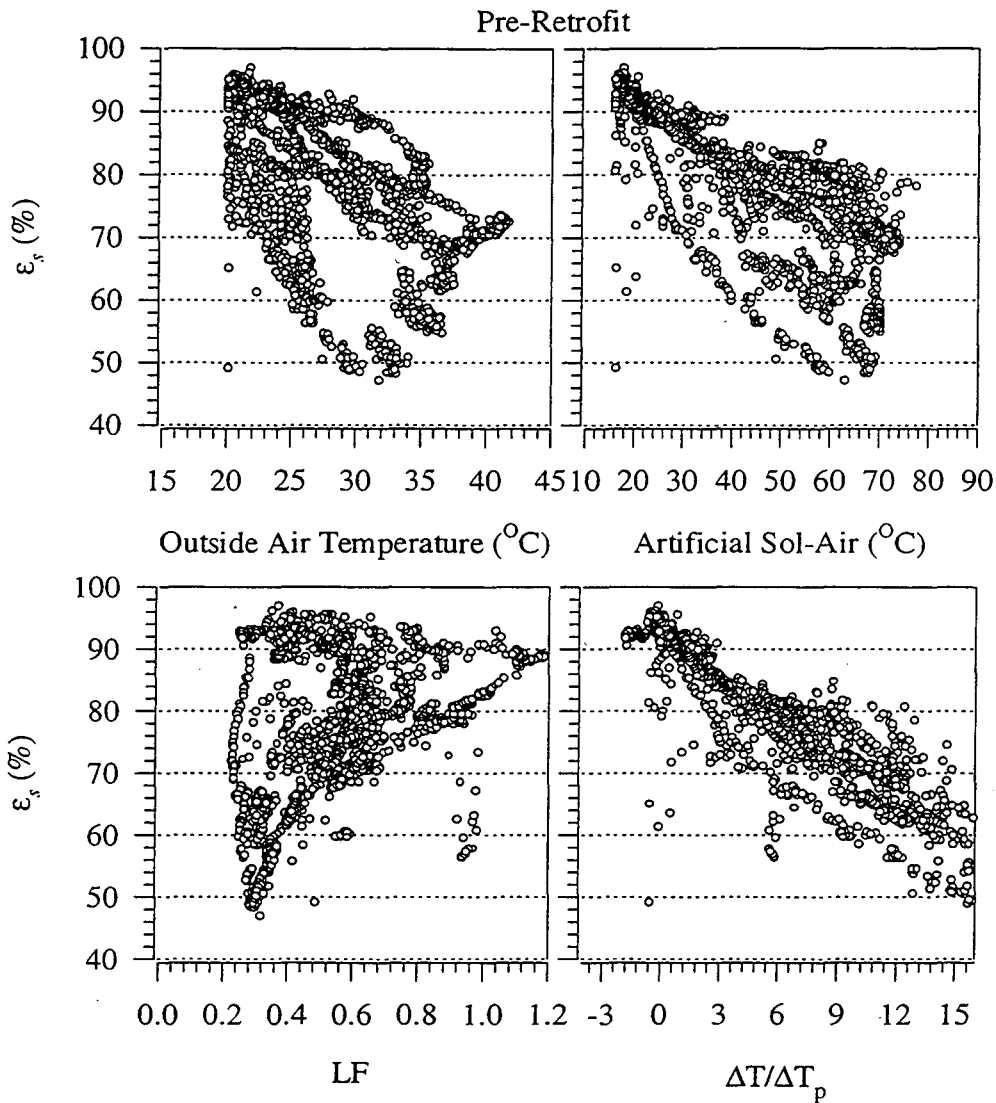


FIGURE 5. Return effectiveness (ϵ_r) vs. outside air temperature, sol-air temperature, load factor and a scaling parameter $\Delta T/\Delta T_p$

4.2.2 Analysis of Measured Results

Figures 6 through 8 present measured results for the supply effectiveness, return effectiveness and delivery efficiency. Pre- and post-retrofit results are shown on each plot. The data collection system collected data regardless of the operating status of the chiller or the air handler. The results in these figures are for normal operating conditions only. The x-axis on each plot is $\Delta T/\Delta T_p$, which is scaled with the artificial sol-air temperature based on the ASHRAE parameters for a light surface. This

removes the effects of different surface properties and ensures that results for comparable operating conditions are compared accurately between the pre and post-retrofit time periods. In each one of these plots, dashed lines bounding each data set indicate the data within the 95th percentile (i.e., 95% of the data). The dashed lines at the core of the data indicate a 95th percentile confidence interval on a first order regression of the data.

4.2.2.1 Measured Supply Effectiveness ϵ_s

Figure 6 plots ϵ_s for both the pre- and post-retrofit cases. The improvement in ϵ_s over the course of the retrofit is obvious at higher values of $\Delta T/\Delta T_p$. At $\Delta T/\Delta T_p = 12$, the pre-retrofit ϵ_s values are grouped around 58% while the post-retrofit values are around 82%. The results are nearly the same (pre- and post-retrofit) at the lower values of $\Delta T/\Delta T_p$, due to the fact that there is little to no conduction gains in this region of the data. At these low temperature differentials the only losses possible are due to leakage, but the retrofit did not change the leakage to any significant degree. For any given $\Delta T/\Delta T_p$, the spread of the ϵ_s data within the 95th percentile was less than 15% for the pre-retrofit and less than 10% for the post-retrofit.

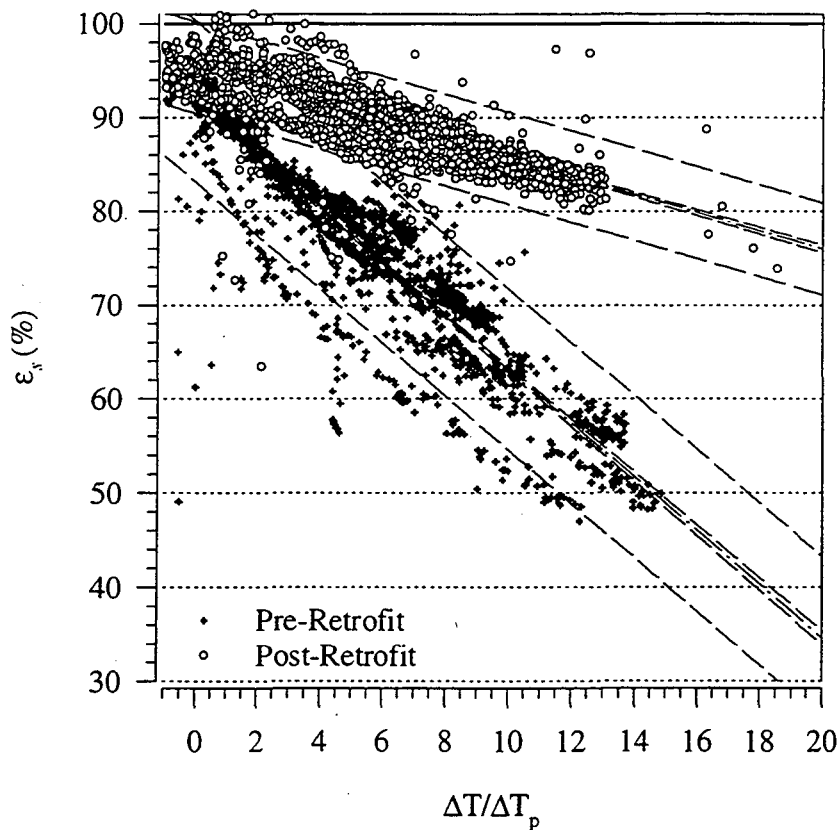


FIGURE 6. Supply effectiveness (ϵ_s) vs. a scaling parameter ($\Delta T/\Delta T_p$)

4.2.2.2 Measured Return Effectiveness ϵ_r

Figure 7 plots the measured return effectiveness, ϵ_r , for both the pre- and post-retrofit cases. The same trends are found as for the ϵ_s , with improved post-retrofit performance at high $\Delta T/\Delta T_p$ values. At $\Delta T/\Delta T_p = 12$, the pre-retrofit values are grouped around 78% while the post-retrofit values are around 94%. The ϵ_r data is not grouped as tightly as ϵ_s data. For any given $\Delta T/\Delta T_p$, the spread of the data within the 95th percentile was less than 18% for the pre-retrofit and less than 22% for the post-retrofit. This grouping of the data can be attributed to changes in the amount of outside air brought into the air handler which affected the amount of return air coming from the space. The overall fan flow was unaffected by changes in the outside air flow, increases in outside air flow were offset by decreases in return grill flow. Decreasing the return grill flow results in lower duct velocities and increased resident times, leading to higher return plenum temperatures. Outside air flow is dependent on the position of the interior and exterior doors which could be (and were) often changed by the occupants independent of any other parameters. This behavior, along with measurement difficulties, is affecting the spread of the ϵ_r data.

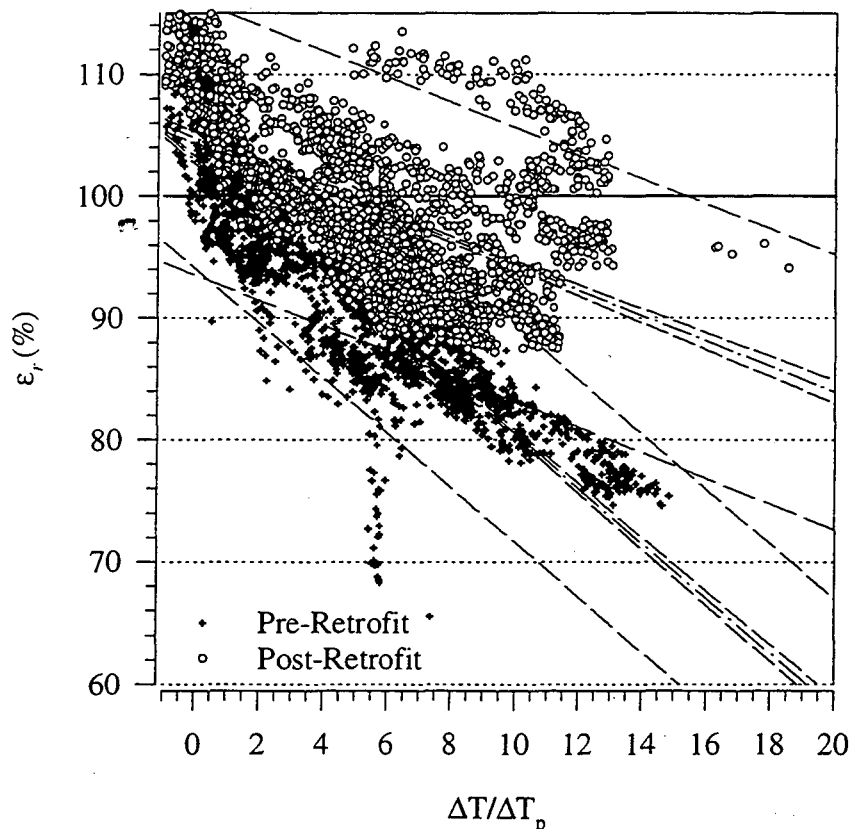


FIGURE 7. Return effectiveness (ϵ_r) vs. a scaling parameter ($\Delta T/\Delta T_p$)

4.2.2.3 Measured Delivery Efficiency η_{del}

Figure 8 plots the measured delivery efficiency, η_{del} , for both the pre- and post-retrofit cases. Since η_{del} is the product of ϵ_s and ϵ_r , the results follow the same trends as the previous plots. When $\Delta T/\Delta T_p = 12$, the pre-retrofit η_{del} is around 45% while the post-retrofit is around 77%. The spread of the data within the 95th percentile was less than 20% for both the pre and post-retrofit cases.

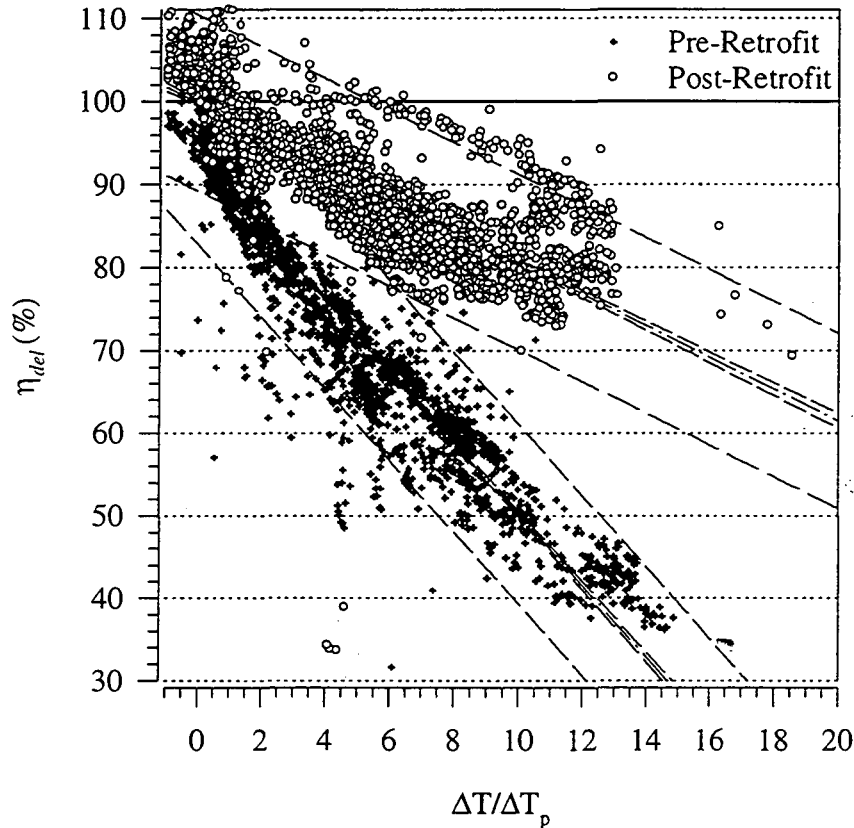


FIGURE 8. Delivery efficiency (η_{del}) vs. a scaling parameter ($\Delta T/\Delta T_p$)

4.2.2.4 Summary of Measured Results

Table 2 presents the average results for each collection period and the percent change with respect to the pre-retrofit case. Despite the fact the ducts had a pre-retrofit conduction efficiency, β , of 97%, the calculated initial average delivery efficiency was only 73%. The retrofit changed β by only 1.7%, but the delivery efficiency changed by 21% of the original value. The uniformly weighted averages are the simple average of the values during each collection period, while the capacity weighted averages weight the values according to the potential cooling capacity when that value was taken.

TABLE 2. Summary of Average Results

	Uniformly Weighted Average			Capacity Weighted Average		
	pre-retrofit	post-retrofit	percent change (post-retrofit in relationship to pre- retrofit)	pre-retrofit	post-retrofit	percent change (post-retrofit in relationship to pre- retrofit)
ϵ_s	78%	90%	15%	80%	90%	13%
ϵ_r	92%	99%	7%	92%	98%	6%
η_{del}	73%	89%	21%	74%	88%	19%

4.2.3 Delivery Effectiveness Model

A model was developed, based on Equations 2 and 3, to calculate the supply and return effectiveness using measured data in cases where a minimum amount of measured data is available (room, supply plenum and return plenum temperatures and percent leakage). This model, represented in Equations 6 and 7, (and derived in Appendix B) can be used to calculate the supply and return delivery effectiveness.

$$\epsilon_s = \alpha_s - \alpha_s (1 - \beta_s) \frac{\Delta T}{\Delta T_p} \quad (6)$$

$$\epsilon_r = \frac{1}{\frac{\Delta T}{\Delta T_p} - \alpha_r \beta_r \left(\frac{\Delta T}{\Delta T_p} - 1 \right)} \quad (7)$$

where:

- α_s = fraction of the fan flow reaching the space
- α_r = fraction of the return plenum flow from the space
- $\Delta T/\Delta T_p$ = scaling parameter (defined in Equation 5)

4.2.3.1 Modeled Results

Equations 6 and 7 are used to model the supply and return effectiveness. The model requires the following information: percent leakage, α ; conduction efficiency, β ; and supply, room, and sol-air temperatures (or more generally, duct ambient temperatures (including solar radiation)). Figures 9 through 11 present the comparisons between the modeled and measured efficiencies, where leakage

values, α 's, and conduction efficiency, β , are from Table 1, while the temperatures were from the monitored data.

4.2.3.2 Comparison Between Modeled and Measured Results

Figures 9 through 11 present the results with the model by plotting modeled values versus measured values. In general, the model did a good job of predicting the results. In some cases the model over-predicted both pre- and post-retrofit efficiencies (i.e., measured values of 38%, predicted values of 89%). For example, in Figure 11 the post-retrofit case has a measured efficiency of 38% while the predicted value was 89%. Returning to Figure 8, it shows that at $\Delta T/\Delta T_p$ near 4 there were efficiencies below 40%. These points are due to system dynamics, e.g., the system being turned on in the middle of the day after it has been off for a while. The model is steady state in nature and will not pick up these kind of system dynamics. This limitation, along with the scatter present in Figures 6 through 8, explain the scatter in Figures 9 through 11.

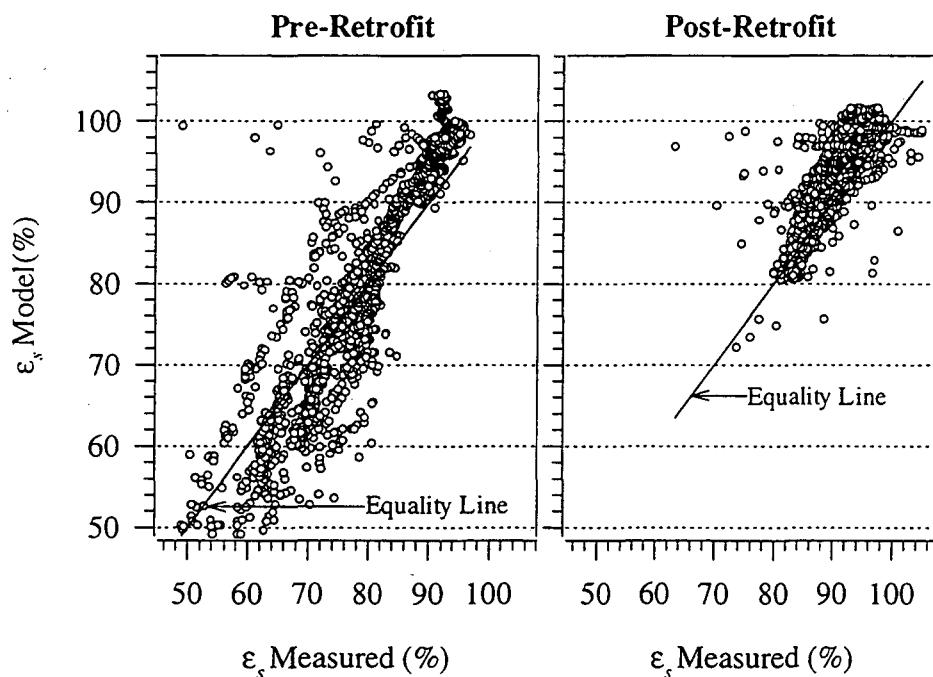


FIGURE 9. Modeled vs. measured supply effectiveness (ϵ_s)

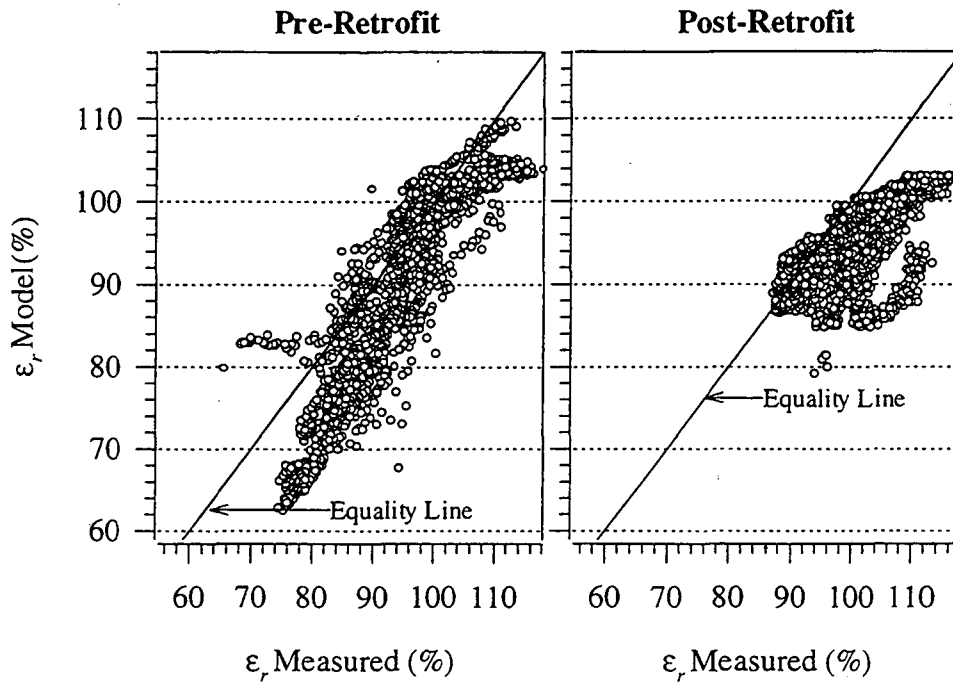


FIGURE 10. Modeled vs. measured return effectiveness (ϵ_r)

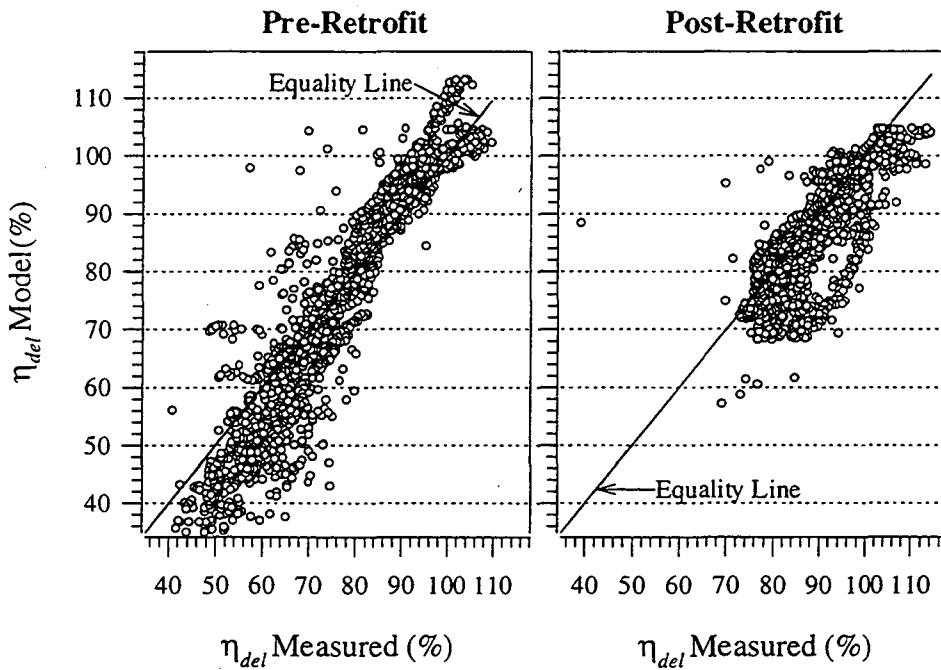


FIGURE 11. Modeled vs. measured delivery efficiency (η_{del})

In Figures 9 through 11, many data points map out to be the same. There might be 100 occurrences of measured and modeled values near 80%, but they appear as a few blurred points. Figure 12 shows the distribution of percent errors of the modeled values with respect to the measured values for the supply effectiveness, return effectiveness and delivery efficiency. The lower and upper caps represent the 10th and 90th percentiles respectively, the lower and upper boundaries of the boxes represent the 25th and 75th percentiles respectively, and the line is the median value. The median error values are closer to zero in the post-retrofit case for both supply and return effectiveness. The median errors for the supply effectiveness are larger than zero and for the return effectiveness less than zero. These errors balance out in the calculation of the delivery effectiveness, with the median error at -3% for both pre and post-retrofit. As the model is a steady-state model and the measured results are from a dynamic system, the spread in the model error is larger and corresponds to the spread found in the measured values.

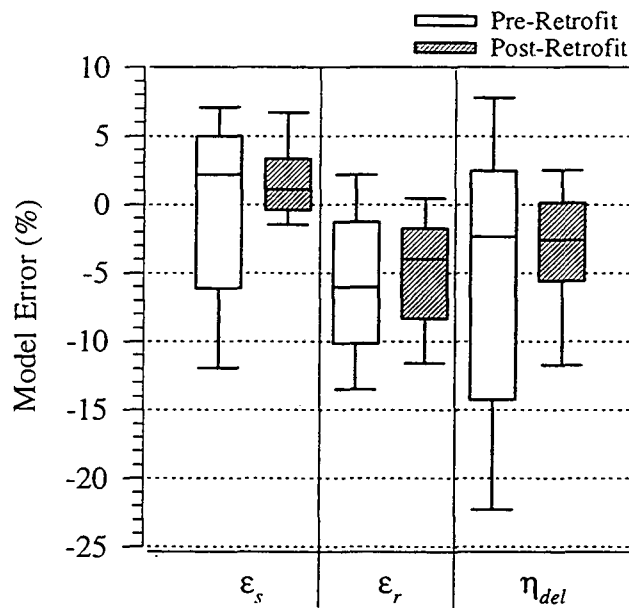


FIGURE 12. Distribution of model errors

Table 3 presents the mean absolute value of the percent error and standard deviation of the model. The highest mean absolute value of the percent error occurred with the pre-retrofit η_{del} data. The model still predicted the results within 10% of the measured results.

TABLE 3. Mean Absolute Value of Percent Error

	Pre-Retrofit		Post-Retrofit	
	Error	Std. Dev	Error	Std. Dev
ϵ_s	7.0	6.5	2.7	3.0
ϵ_r	6.8	5.1	5.7	6.2
η_{del}	10.2	9.8	5.1	7.8

4.3 Effect of Reflective Coating on the System Performance

The “Cool-Roof” retrofit reduced the average HVAC system energy use by 22%. This reduction was due partly to the added insulation and partly to the reflective coating. Using the model presented in Appendix B, it is possible to separate out the influences of the insulation and that of the reflective coating. The additional insulation only affects the conduction effectiveness, β , while the application of the reflective surface changes the sol-air temperature which affects only the $\Delta T/\Delta T_p$. Modeling the post-retrofit time period with the changed β and both pre and post-retrofit reflectivity values separates out the effect of the added insulation from the full retrofit. Both the measured and modeled results show that the full retrofit increased the average delivery efficiency, η_{del} , by 21% of the original value, while the model predicted that the average change in η_{del} due to insulation alone was 14% of the original value. The remainder of the change in the η_{del} is attributed to the increased reflectivity of the surface. Figure 13 shows the results of the model when η_{del} is determined for the three conditions (pre-retrofit, insulation only and post-retrofit) using a wide range of $\Delta T/\Delta T_p$ values, assuming the reflectivity and insulation values measured for each condition. The same ambient conditions (outside air temperature, and incident solar radiation) and load factors (i.e., room temperature) were used in all three cases. The conduction effectiveness, β , and the surface reflectivities are specific to each condition. This presentation of the data provides a clear interpretation of the specific retrofit activities’ effects on the delivery effectiveness.

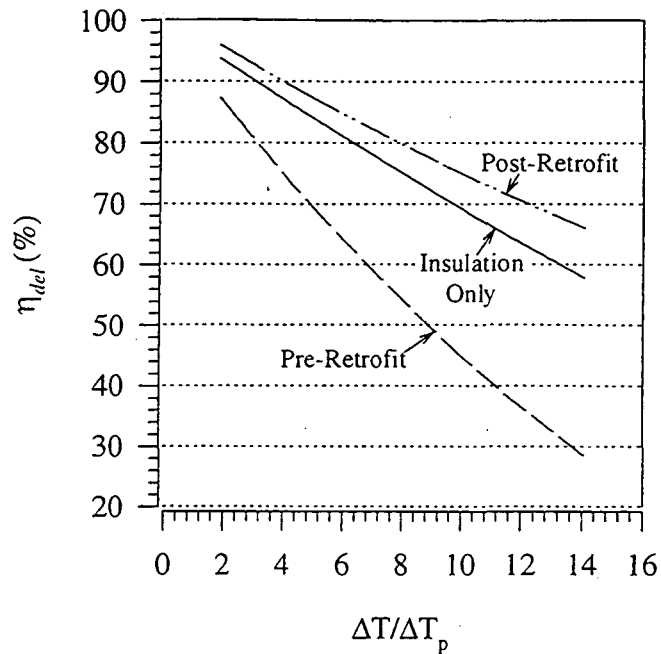


FIGURE 13. Different Parts of the Retrofit on η_{del}

4.4 Impacts of Retrofit on Thermal Comfort

Conduction losses, in cooling mode, raise the supply air temperature. An increase in supply temperature presents a thermal comfort issue, especially in systems with duct runs having different lengths. With long lengths of ductwork serving zones isolated from the thermostat, problems arise with uneven temperature distribution in the rooms served by the system. The length of the duct runs to each supply register in the system studied had lengths of 12.2 m (40 ft), 18.3 m (60 ft), 5.5 m (18 ft), and 11.6 m (38 ft) each. Figure 14 shows a regression fit of the measured temperature rise for each register. The register nearest the air handler, having the shortest duct run and residence time, experienced the lowest temperature rise while the register furthest away from the air handler, having the longest duct run and residence time, experienced the greatest temperature rise. For an extreme condition of $\Delta T / \Delta T_p = 15$, pre-retrofit, the shortest run had a rise of 1.0°C and the longest run had a rise of 2.4°C . For post-retrofit at the same conditions, the shortest run had a rise of 0.2°C and the longest run had a rise of 0.7°C .

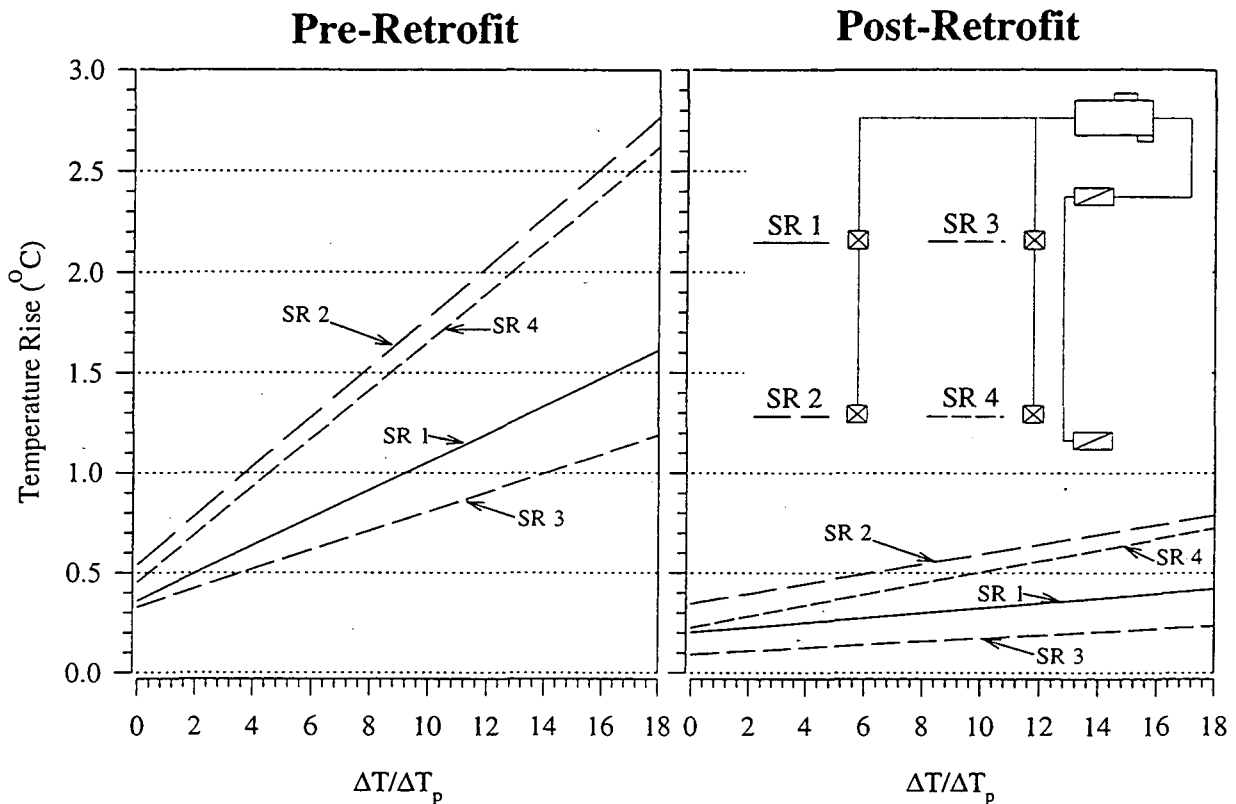


FIGURE 14. Temperature Rise At Registers

Corresponding to the temperature drops through the duct runs, Figure 15 shows the percentage of the cooling potential of the air entering the supply plenum. The capacity loss for each register is calculated according to Equation 8.

$$CapacityLoss_i = 1 - ((T_i - T_{room}) / (T_{supply} - T_{room})) \quad (8)$$

For the same extreme condition of $\Delta T / \Delta T_p = 15$, pre-retrofit, the shortest run had a capacity loss of 31% and the longest run had a capacity loss of 70%. For the same conditions in the post-retrofit period, the shortest run had a capacity loss of 9% and the longest run had a capacity loss of 31%. Significant losses occur even though the conduction effectiveness of ducts were 0.969 (pre-retrofit) and 0.985 (post-retrofit). This condition is due to the high loss potential when the sol-air temperature rises to 60°C as well as the fact that β_s scales with the difference between the sol-air and supply duct

temperatures while the capacity losses scale with the difference between the room and supply duct temperatures.

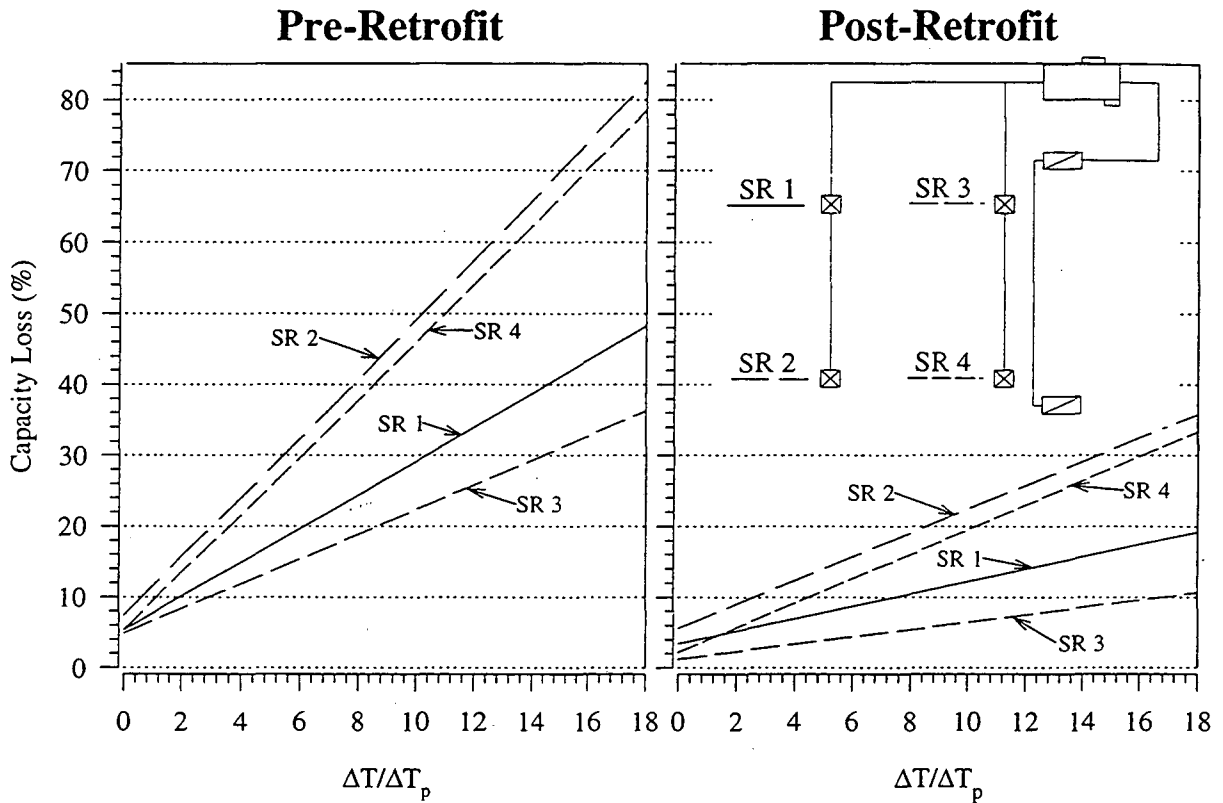


FIGURE 15. Capacity loss at registers

Table 4 summarizes the measured conduction losses for each register. As in Table 2, the uniformly weighted averages are the simple average of the values during each collection period, while the capacity weighted averages weight the values according to the potential cooling capacity when that value was taken.

4.5 Effect of “Cool-Roof” Retrofit on System Operating Conditions

The artificial sol-air temperature and the system load factor, LF, can be used to compare the system operating conditions between the pre and post-retrofit monitoring periods. Using a box plot, Figure 16 shows a comparison of these two main factors and shows that the two monitoring periods had similar weather conditions. As the artificial sol-air temperature is a function of the weather, both the pre- and post-measuring periods had similar median artificial sol-air temperatures. The load factor

TABLE 4. Summary of Average Register Conduction Losses

Supply Register	Uniformly Weighted Average			Capacity Weighted Average		
	pre-retrofit Capacity Loss	post-retrofit Capacity Loss	percent change (post-retrofit in relationship to pre-retrofit)	pre-retrofit Capacity Loss	post-retrofit Capacity Loss	percent change (post-retrofit in relationship to pre-retrofit)
1	17%	9%	-46%	16%	9%	-47%
2	27%	16%	-41%	25%	15%	-40%
3	14%	5%	-64%	13%	5%	-64%
4	25%	13%	-48%	23%	12%	-45%

(LF) depends on the internal loads, the building shell load, and η_{del} . The lecture hall had similar occupancy schedules, class sizes and utilization during both monitoring periods. Therefore, it appears the changes in the LF are due to the retrofit project.

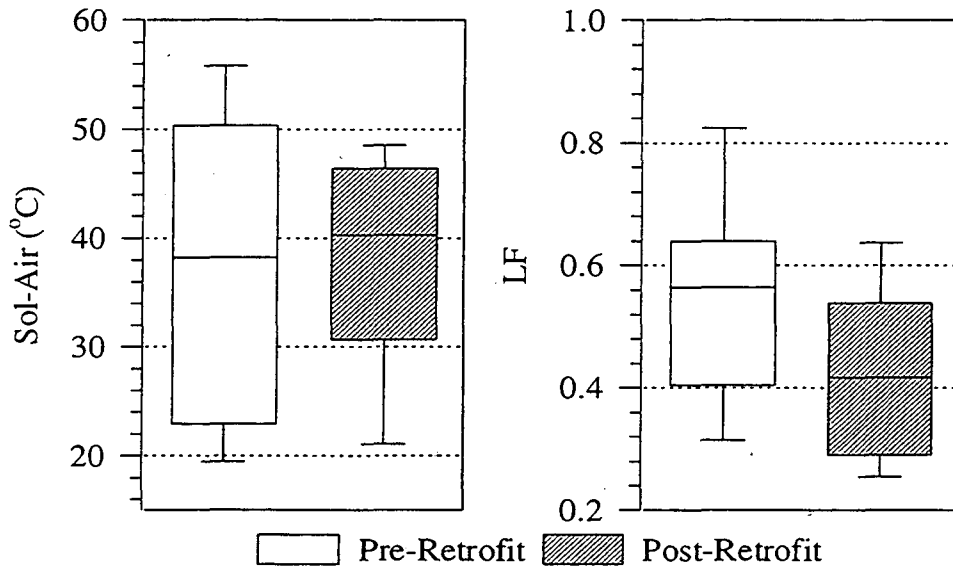


FIGURE 16. Operating Conditions - Pre and Post-Retrofit

Table 5 summarizes the system impacts of the retrofit project. The average load factor, LF, decreased by 22%, which is the same as the reduction in the amount of energy used by the system. Average duct losses decreased by 1.4kW, which corresponds to a 67% reduction. The average energy delivery rate to the space (energy delivered to the space from the registers) decreased by only 0.4kW. The ΔT in Table 5 represents the potential temperature difference across the roof. It is the temperature difference between the light colored artificial sol-air and the room temperature. The average potential across the roof increased by 3%. Since the internal loads in the space were similar for both

measurement periods, the load decrease in the space is attributable to the roof changes. Even accounting for the slightly increased potential gains due to the slightly higher potential ΔT , the roof changes contributed to no more than an average decrease in load of 0.5kW between the pre- and post-retrofit measurement periods. This shows that the average saving was approximately 2kW, of which 75% is attributable to the duct changes. Even though the surface area of the supply ducts are only 31% of the area of the roof, they represent a greater percentage of the savings.

TABLE 5. Summary of Average Losses, LF, and Delivered Energy

	Pre-retrofit	Post-retrofit	Change
η_{del}	73%	89%	21%
Load Factor (LF)	56%	44%	-22%
Duct Losses	2.1 kW	0.7 kW	-67%
Energy Delivery Rate	5.8 kW	5.4 kW	-6%
ΔT (across roof) ^a	15.2 °C	15.7 °C	3%

^a $T_{sol-air} - T_{light\ surface} - T_{room}$

5.0 Conclusions

With exterior ducts, large thermal losses are present even in systems which are believed to be “good systems” (e.g., low leakage and silver painted ducts). This condition is due to: 1) for ducts directly exposed to sunlight, the conduction losses scale with the sol-air temperature and 2) any thermal losses are completely lost to outside. In order to decrease losses, systems with exterior ducts have to have lower levels of leakage and more insulation than those with ducts located entirely inside the building or conditioned space. This study showed that the application of added insulation and a reflective coating proved beneficial in reducing the thermal losses of rooftop exposed ductwork, reducing the average system energy use by 22%, 16% due to the duct improvements and 6% due to the roof improvements. Due to the fact that the building shell load is usually a relatively small percentage of the overall system load, duct retrofits are likely to have a greater impact than roof retrofits on commercial buildings with exterior ductwork.

The effectiveness calculation methodology described and used in the analysis of this project allows separate investigation of individual components in a delivery system. This methodology can be used in analyzing a wide variety of ductwork systems, as supply and return effectiveness are calculated independently of each other and then combined to calculate the system delivery efficiency. This method allows analysis of commercial systems containing outside air and economizer features, without the outside air incurring an artificial penalty as a “return leak.” This model works equally well with ducts not located on the roof, although such cases would need to account for thermal recovery.

The steady-state model predicts the results with reasonable accuracy, allowing investigation of a wide range of "what-if" retrofits. By referencing the weather and system operating conditions, the model predicts the effectiveness of the ducts. With minor modifications, the model can report the effectiveness of individual pieces of the delivery system. This model provides a tool which could be used to predict which systems, and even which part of systems, would benefit most from retrofitting. This tool could be used by the design community in evaluating the impact of various proposed thermal distribution systems, allowing designers to model improvements to their designed systems to minimize estimated thermal loss impacts. This simplified model can also be used by engineers, designers and energy management personnel to verify the performance and to pinpoint areas for energy improvement efforts for new and existing thermal distribution systems.

6.0 Acknowledgments

The research reported here was jointly funded by the California Institute for Energy Efficiency (CIEE), under Contract No. B93-05A, and by the Assistant Secretary for Energy Efficiency and Renewable Energy, Office of Buildings and Community Systems of the U.S. Department of Energy, under Contract No. DE-AC03-76SF00098.

The authors would like to thank Joe Bardon, Los Rios Community College District; Bruce Vincent, Sacramento Municipal Utility District; Karl Brown, California Institute for Energy Efficiency; and Hashem Akbari, Lisa Gartland and Rick Diamond of Lawrence Berkeley National Laboratory.

7.0 References

- Akbari, H., Bretz, S., Hanford, J., Kurn, D., Fishman, B., Taha, H., and Bos, W.; "Monitoring Peak Power and Cooling Energy Savings of Shade Trees and White Surfaces in the Sacramento Municipal Utility District (SMUD) Service Area: Data Analysis, Simulations, and Results, Berkeley, CA," Lawrence Berkeley National Laboratory, LBL-34411, 1993.
- ASHRAE Standard 62, Ventilation for Acceptable Indoor Air Quality, American Society of Heating, Refrigerating and Air conditioning Engineers, 1989a.
- ASHRAE Handbook of Fundamentals, American Society of Heating, Refrigerating and Air Conditioning Engineers, 1989b.
- Modera, M.P., Feustel, H.E., Matson, N.E., Huizenga, C., Bauman, F., Arens, E. and Borgers, T.; "Efficient Thermal Energy Distribution in Commercial Buildings," Report to the California Institute for Energy Efficiency, May 1996 (draft).

Appendix A

Fan Flow Measurement Using a Constant Injection Tracer Gas Technique

A.1. Setup

1. Place end of the sampling tube at the face of a supply register.
2. Set the tracer gas injection tube outlet inside a return register.
3. Start injecting the tracer gas at a constant rate.
4. Write down concentration rate readings.
5. Stop injecting when the concentration rates level off (approximately 10 minutes).
6. Continue taking concentration readings for 10 more minutes.

A.2. Analysis

This method assumes the following:

- The background (outside) tracer gas concentration is negligible.
- Sufficient mixing occurs across the fan and equipment such that the concentration is uniform throughout the supply system.

Ideally tracer gas tests should use two analyzers, one upstream of the injection location and one downstream. With commercial buildings this is not easily done, since outside air dampers are present immediately upstream of the fan, making accurate upstream concentration measurements difficult/impossible. Since the return side operates under a negative pressure (with respect to outside), leaks and outside air will decrease the concentration. The supply side always operates under a positive pressure (with respect to outside), so leaks do not change the concentration. The concentration at the supply during injection is given according to Equations 1.

$$C_1(t) = \frac{\dot{V}_{inj} + \dot{V}_{room}(t) + \dot{V}_{outside}}{\dot{Q}_{fan}} \quad (A1)$$

The concentration at the supply after injection is given according to Equations 2.

$$C_2(t) = \frac{\dot{V}_{room}(t)}{\dot{Q}_{fan}} \quad (A2)$$

where:

- \dot{V}_{inj} = Volumetric flowrate of tracer injected in the return
 $\dot{V}_{room}(t)$ = Volumetric flowrate of tracer entering from the room at time t
 $\dot{V}_{outside}$ = Volumetric flowrate of tracer entering from outside = 0
 \dot{Q}_{fan} = Volumetric flowrate of the fan
 $C(t)$ = Concentration measured at the supply at time t

At the instant injection is stopped, the $\dot{V}_{room}(t)$ in both Equations 1 and A2 are the same. Substituting Equations 2 into A1 yields the following relationship for \dot{Q}_{fan} .

$$\dot{Q}_{fan} = \frac{\dot{V}_{inj}}{C_1(t_{off}) - C_2(t_{off})} \quad (A3)$$

where:

t_{off} = time when the injection was turned off

Care is required in obtaining values for C_1 and C_2 . C_1 is usually from clean data where little is required other than reading the value. However if the data is not perfect, characterizing the charge up and using the point from the characterization may be required. Due to the response of the analyzer and the distribution of the tracer gas, C_2 , cannot be directly read at the time injection stops. Assuming data is collected at 15 second intervals, the first three or four points are thrown out. Using the rest of the data, an exponential decay is characterized and the value for t_{off} is back extrapolated from this. Figure A17 illustrates an example of a data set obtained from the building.

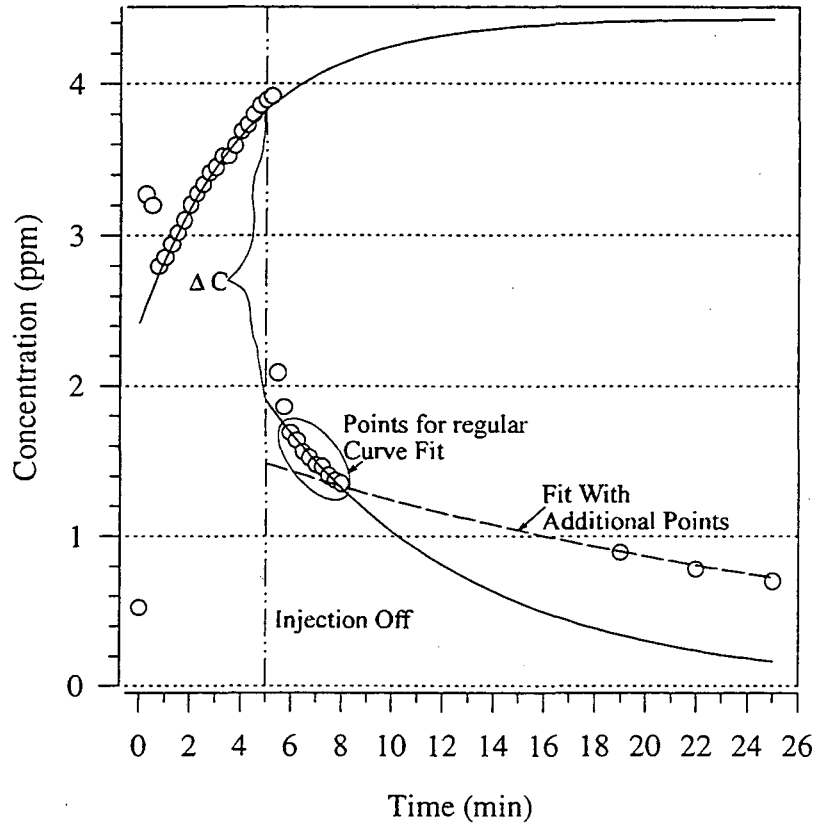


FIGURE 17.Example data

Appendix B

Model for Delivery Effectiveness and Efficiency Calculations

B.1. Background

Figure B18 shows a general schematic for the type of system studied with this model. With the exception of the α terms, most variables and parameters should be self explanatory.

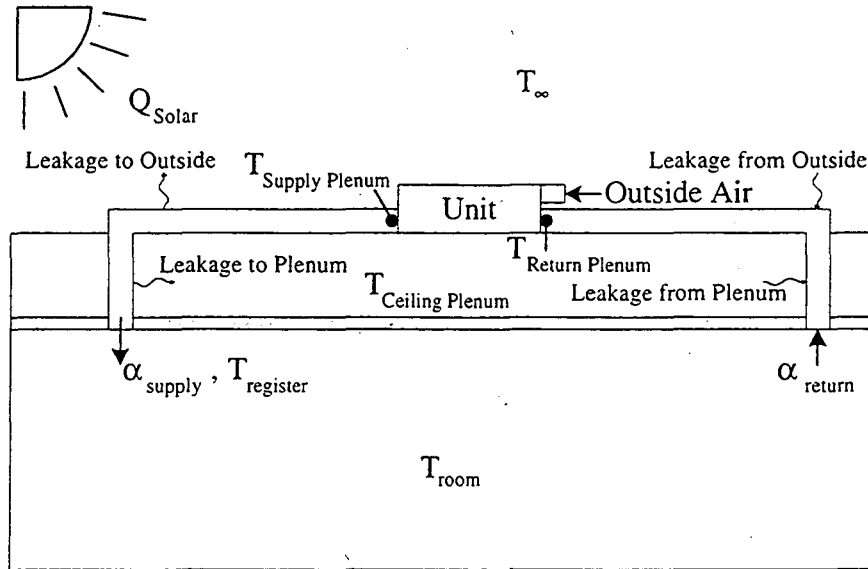


FIGURE 18. General System Schematic

Equation 1 defines α_s as the fraction of fan flow to the flow to the supply registers.

$$\alpha_s = \frac{\dot{m}_{supply}}{\dot{m}_{fan}} \quad (B1)$$

Equation 2 defines α_r as the fraction of fan flow to the flow from the return registers.

$$\alpha_r = \frac{\dot{m}_{return}}{\dot{m}_{fan} - \dot{m}_{OutsideAir}} \quad (B2)$$

B.2. Conduction Efficiency

Conduction efficiency relates the temperature change in a duct to the physical properties of the duct. To start define a duct segment in an infinite surroundings (heat transfer to/from the duct does not change the temperature of the surroundings), Figure B19 schematically defines just such a segment.

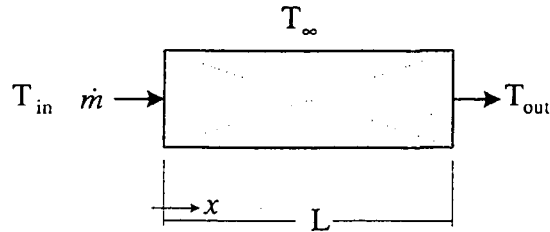


FIGURE 19. Duct segment

Writing a heat balance for a differential duct element yields Equation B3.

$$UdA(t - T_{\infty}) = -\dot{m}C_p dt \quad (\text{B3})$$

which can be written as:

$$\frac{UP}{\dot{m}C_p} dx = \frac{dt}{(t - T_{\infty})} \quad (\text{B4})$$

Integrating over the length of the duct segment,

$$-\int_0^L \frac{UP}{\dot{m}C_p} dx = \int_{in}^{out} \frac{dt}{(t - T_{\infty})} \quad (\text{B5})$$

yields:

$$-\frac{UPL}{\dot{m}C_p} = \ln\left(\frac{T_{out} - T_{\infty}}{T_{in} - T_{\infty}}\right) \quad (\text{B6})$$

or:

$$\exp\left(-\frac{PL}{\dot{m}C_pR}\right) = \left(\frac{T_{out} - T_{\infty}}{T_{in} - T_{\infty}}\right) \quad (B7)$$

The conduction efficiency, β , can be defined as:

$$\beta \equiv \left(\frac{T_{out} - T_{\infty}}{T_{in} - T_{\infty}}\right) \quad (B8)$$

Substituting Equation B8 into Equation B7 yields the relationship between the conduction efficiency and the physical properties of the duct, as shown in Equation B9.

$$\beta = \exp\left(-\frac{PL}{\dot{m}C_pR}\right) \quad (B9)$$

where:

- P : The perimeter of the duct
- L : Length of the duct
- \dot{m} : The mass flow rate of air through the duct
- C_p : The specific heat of air
- R : The thermal resistance of the duct = $1/U$

Thus the conduction efficiency is a function of the duct properties and not the ambient surroundings. A duct with an infinite thermal resistance has a β of unity, the temperature of the air in the duct does not change. While a duct with no resistance has a β of zero, the temperature leaving the duct is equal to the temperature of the surroundings.

B.3. Supply Effectiveness

The supply effectiveness is a measure of the supply system. It is the ratio of the capacity supplied by the ductwork to the space to the potential capacity put into the supply at the plenum.

$$\epsilon_s \equiv \frac{\text{Delivered}}{\text{Potential}} = \frac{\alpha_s (T_{reg} - T_{room})}{(T_{supply} - T_{room})} \quad (\text{B10})$$

By using Equation B8, setting T_{reg} equal to T_{out} and T_{supply} equal to T_{in} and assuming that all the supply leaks occur at the end of the ducts, one arrives at:

$$T_{reg} = \beta_s (T_{supply} - T_\infty) + T_\infty \quad (\text{B11})$$

Substituting this into Equation B10 we get:

$$\epsilon_s = \frac{\alpha_s (\beta_s (T_{supply} - T_\infty) + T_\infty - T_{room})}{(T_{supply} - T_{room})} \quad (\text{B12})$$

Equation B12 can be written as:

$$\epsilon_s = \frac{\alpha_s \beta_s (T_{supply} - T_\infty) + \alpha_s (T_{supply} - T_{room}) - \alpha_s (T_{supply} - T_\infty)}{(T_{supply} - T_{room})} \quad (\text{B13})$$

Now the following parameter can be introduced,

$$\frac{\Delta T}{\Delta T_p} = \frac{(T_{supply} - T_\infty)}{(T_{supply} - T_{room})} \quad (\text{B14})$$

Substituting Equation B5 into Equation B13 yields:

$$\epsilon_s = \alpha_s - \alpha_s(1 - \beta_s) \frac{\Delta T}{\Delta T_p} \quad (\text{B15})$$

B.4. Return Effectiveness

A similar approach works for the return system. The return effectiveness is the ratio of the minimum energy required to condition the space to the actual energy.

$$\epsilon_r \equiv \frac{\text{Ideal}}{\text{Actual}} = \frac{(T_{\text{supply}} - T_{\text{room}})}{(T_{\text{supply}} - T_{\text{ret}})} \quad (\text{B16})$$

Assuming the leakage is at the return register (the beginning of the return duct). Equation B17 is the adiabatic mixing temperature used for the T_{in} in Equation B8.

$$T_{in} = \alpha_r T_{room} + (1 - \alpha_r) T_{\infty} \quad (\text{B17})$$

This yields the following for T_{ret} :

$$T_{ret} = \alpha_r \beta_r (T_{room} - T_{\infty}) + T_{\infty} \quad (\text{B18})$$

Substituting Equation B18 into Equation B3 yields:

$$\epsilon_r = \frac{(T_{\text{supply}} - T_{\text{room}})}{(T_{\text{supply}} - \alpha_r \beta_r (T_{\text{room}} - T_{\infty}) - T_{\infty})} \quad (\text{B19})$$

This can be written as:

$$\epsilon_r = \frac{1}{\left(\frac{T_{supply} - T_{\infty}}{T_{supply} - T_{room}}\right) - \alpha_r \beta_r \left(\frac{T_{room} - T_{\infty}}{T_{supply} - T_{room}}\right)} \quad (B20)$$

or:

$$\epsilon_r = \frac{1}{\frac{\Delta T}{\Delta T_p} - \alpha_r \beta_r \left(\frac{T_{room} - T_{\infty} + T_{supply} - T_{supply}}{T_{supply} - T_{room}}\right)} \quad (B21)$$

Which reduces to the final relationship for the return effectiveness:

$$\epsilon_r = \frac{1}{\frac{\Delta T}{\Delta T_p} - \alpha_r \beta_r \left(\frac{\Delta T}{\Delta T_p} - 1\right)} \quad (B22)$$

B.5. Delivery Efficiency

The potential capacity put into the supply at the plenum is the same as minimum energy required to condition the space. This allows combing the effectiveness yielding the distribution delivery efficiency. This efficiency is defined as the ratio of the energy delivered by the duct system to that supplied to the duct system.

$$\eta_{del} \equiv \frac{\text{Delivered}}{\text{Actual}} = \epsilon_s \cdot \epsilon_r \quad (B23)$$

Which is:

$$\eta_{del} = \frac{\alpha_s - \alpha_s(1 - \beta_s) \frac{\Delta T}{\Delta T_p}}{\frac{\Delta T}{\Delta T_p} - \alpha_r \beta_r \left(\frac{\Delta T}{\Delta T_p} - 1 \right)} \quad (\text{B24})$$

**ERNEST ORLANDO LAWRENCE BERKELEY NATIONAL LABORATORY
ONE CYCLOTRON ROAD | BERKELEY, CALIFORNIA 94720**